Neuronal cultures grown on patterned substrates: impact of neuron's origin

Author: Laia Romeu Casas
Facultat de Física, Universitat de Barcelona, Diagonal 645, 08028 Barcelona, Spain.

Advisor: Jordi Soriano i Fradera

Abstract: We studied the dynamics observed in neuronal cultures derived from two different rodent species. Neurons in culture grew on a topographically-modulated substrate with a fractal-like shape that facilitated an intricate connectivity between neurons. We observed through fluorescence imaging that this constraint affected the activity of the network, with substrates with fractal pattern substantially reducing the propagation velocity of activity in the network. Additionally, neuronal cultures from mice exhibited greater activity richness and lower velocity than rats' ones. To further explore these results, we employed power spectrum analyses on the recorded data and concluded that it only provided a qualitative insight, without capturing key characteristics. Finally, simulations were conducted to show that the behavior of the two rodent species could be attributed to differences in axonal length under identical maturation conditions.

I. INTRODUCTION

The use of neuronal cultures to study the dynamics and connectivity of neuronal networks has long been a well-established area of research [1]. This experimental technique is particularly noteworthy not only because it offers a simplified and accessible way of examining living neuronal networks, but also because these neuronal networks are active by themselves, exhibiting strong spontaneous activity [2]. This spontaneity means that neurons can self-activate in the absence of any external stimulation, being driven by just inherent noise and fluctuations.

However, these cultures do not exhibit the complexity observed in the human brain [3]. Making cultures closer to the brain is important for modeling diseases *in vitro* and to understand the building blocks governing brain's complexity [1]. To address this effort, various modifications can be implemented into the neuronal cultures to enhance their richness, including chemical stimulation and alterations to the substrate on which the neurons are cultured [4]. This study focuses on the latter approach.

Neuronal cultures are typically derived from rodent sources; however, the behavior of the culture can vary depending on the species of origin. Consequently, a central focus of the present study is to compare the general dynamics of rodent cultures, namely from mice or rats, and examine how the introduction of alterations in the substrate where neurons grow influences this dynamics.

II. MATERIALS AND METHODS

A. Neuronal cultures grown on PDMS surface

The data analyzed in this study were obtained from neuronal cultures derived from primary cortical neurons, and either from rats and mice. These cultures were grown on both standard flat surfaces and polydimethylsiloxane (PDMS) substrates with a topographical modulation made of square patterns that emerged from the surface (Fig. 1A). The sizes of the valleys covered various sizes with a fractal-like organization. All cultures were 6 mm in diameter regardless the surface were neurons grew.

PDMS is a silicon-based organic polymer that serves as a substrate for neuronal cultures. The fractal patterns were imprinted onto the PDMS using a negative mold made of resin, creating a PDMS substrate with elevated reliefs that were intended to break the spatial isotropy of a standard flat surface, in the sense that neurons had to connected to one another through intricate paths. By introducing these spatial and physical constraints, we aim to investigate how the collective behavior of neuronal ensembles is altered and to compare the differences between the neuronal cultures of the two rodent species.

B. Calcium fluorescence imaging

Neurons were cultured at day *in vitro* (DIV) 0, and maintaned with different nutrients in an incubator at 37°, 95% humidity and 5% CO_2. By DIV 5, spontaneous activity emerged on the neuronal cultures, which could be recorded by using calcium fluorescent imaging. In this technique, neurons were infected first with adeno-associated viruses (AAVs) carrying the GCaMP6s calcium sensor gene. This gene expresses the fluorescent calcium indicator as far as the neurons are alive, allowing the detection of changes in intracellular calcium concentrations resulting from neuronal activations, which can subsequently be recorded with a camera in Soriano's Lab and analyzed in a computer.

Although spontaneous activity emerged by DIV 5, GCaMP6s expression was not sufficiently strong for reliable imaging until DIV 6. Consequently, all data discussed here are from DIV 6 and 7. While data from more mature cultures could be obtained, past DIV 7, the neuronal system became increasingly interconnected (as axons grew) [4], leading to a reduction in the variability and richness of the spontaneous activity and that is the focus of this study.

C. Data Analysis

• **Activity events detection.** Calcium imaging recordings were analyzed using the specialized software NETCAL, which can extract the fluorescent time signals from the cultures. Upon importing a given recording into NETCAL, we defined a 6 mm diameter circular grid of regions of interest (ROIs). Although each ROI typically contained a small group of neurons, each ROI was treated for clarity as if it represented a single neuron.

Using NETCAL, the average fluorescence trace of each ROI was extracted, corrected, and normalized. Neuronal activity spikes were subsequently identified using the Schmitt method, which detects rapid changes in fluorescence. The resulting data was presented as a binary map, known as raster plot, where a value of 1 indicates the detection of a spike and a 0 indicates no spike, thus representing the time series of the neuronal activity recorded (Fig. 1B).

• **Burst detection.** When neuron spontaneously activate, they can generate a propagating wavefront across the culture. If the amount of neurons that contribute to this front encompass a large fraction of the culture, one says that a *network burst* has been generated. From a raster plot we can obtain this fraction of the network that activates almost together in a short time window. In the present study, we define a network burst if the network fraction activated in a 100 ms time window and encompasses more than 5% of the network.

When all the bursts on a calcium imaging fluorescence recording are defined, we can calculate some of its properties. By analyzing the positions of each ROI and their respective activation times with Dr. Soriano's laboratory software, it is possible to approximate the origin of this wavefront. Additionally, by measuring the Euclidean distance and time span between each activated ROI, relative to the previously defined activity origin, we can compute the propagation velocity of the wavefront. Moreover, We can evaluate the bursts size, also defined as population activity, A, i.e., the fraction of the network that coactivated together.

D. Network simulation

To quantitatively investigate the differing behaviors observed in rat and mouse neuronal cultures, we used a simulation of a network consisting of 900 neurons. This network was modeled using the Eugene M. Izhikevich mathematical framework [5], which accurately describes the spiking and bursting behavior of neurons. The dynamics of the system are governed by the following differential equations:

$$\frac{dV_m}{dt} = 0.04V_m^2 + 5V_m + 140 - u + I,$$
$$\frac{du}{dt} = a(bV_m - u),$$

where V_m represents the neuron's membrane potential and u a variable for membrane recovery, which account for the activation and inactivation of sodium and potassium currents, respectively, and that are the main drivers of neuronal spike emission and subsequent reset.

The parameters a, b, c and d can be adjusted to represent the desired neuronal behavior within the network:

- a defines the recovery time scale of u, indicating how quickly u returns to its resting state after a spike.
- b determines the sensitivity of u to the membrane potential V_m.
- c and d are the reset values of V_m and u after a spike, respectively.

When V_m exceeds a potential threshold (typically 30 mV), V_m is reset to c and u is increased by d to account for the spike's effect. This resetting mechanism ensures that V_m and u appropriately reflect the neuron's behavior after each spike.

In the present study, all the parameters were maintained constant as in Ref. [5] and we considered as key ingredient the connectivity matrix $S = \{s_{ij}\}$, with $s_{ij} = 1$ if neurons i and j connect, and 0 otherwise. This matrix was constructed as a *random geometric graph*, i.e., by placing neurons on a substrate and connecting any two neurons whose Euclidean distance was below a distance r. In this way, we could study how the activity of a network could change depending on r, which can be understood as the axon length. One could hypothesize, for instance, that rat cultures had a higher r (and therefore stronger connectivity) than mouse cultures. As a result, we could investigate if the different behaviors observed in the experiments were caused by a different axonal length between the two rodent species analyzed at the same maturation day.

III. RESULTS AND DISCUSSION

A. Spontaneous Activity

We prepared neuronal cultures that grew either on a flat surface ('control', Fig. 1A, left) or on a PDMS topographical substrate ('squares', Fig. 1A, right). By observing the spontaneous activity of the networks, its collective behavior could be evaluated. To quantify it, we calculated the population activity, A, extracted from the raster plots, as shown in Fig. 1B. Population activity is the fraction of the network that activates simultaneously, with values from 0.05, when few neurons activate, to 1, when all neurons coactivate.

As expected, control rat cultures exhibit highly coherent behavior, characterized by periods where the majority of neurons activate together, followed by silent intervals. This behavior results in large network bursts

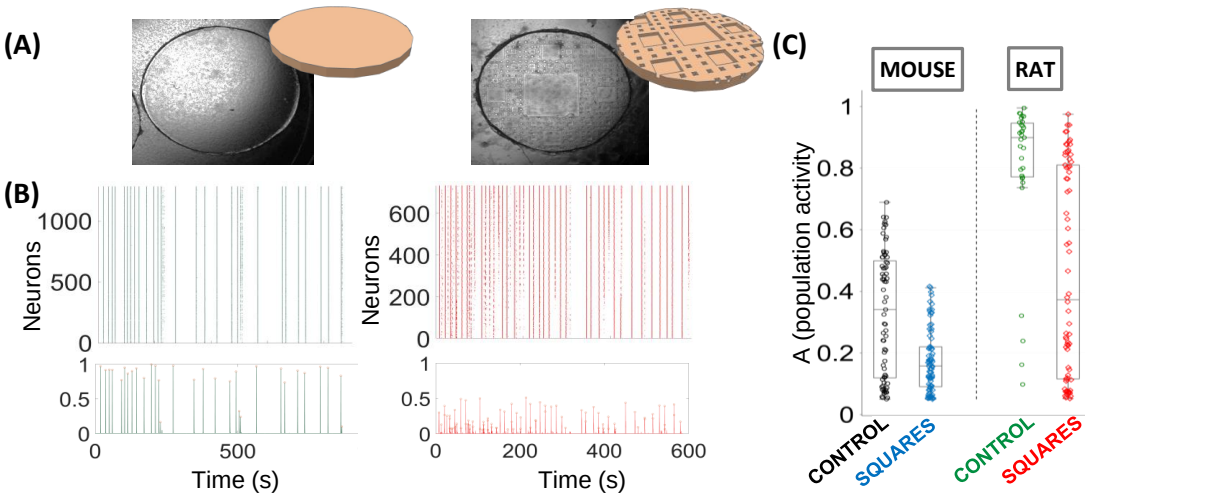

FIG. 1: Spontenous Activity of both mice and rat neuronal cultures grown on PDMS' topographical surfaces. **(A)** Illustrative fluorescence example images of the flat (left) and square valleys (right) topographical designs, referred to as CONTROL and SQUARES, respectively. All cultures were 6 mm in diameter and were recorded on DIV 6 or 7. **(B)** Raster plot (top) and Population Activity (bottom). Each point of the raster represents an ROI activation, while each peak in the population activity represents a burst. **(D)** Distribution of the network fraction that activated in each burst for the four studied systems. Each dot is a burst, and two different cultures are included in each distribution.

size, $\langle A \rangle \simeq 0.9$. In contrast, rat cultures grown in a squared fractal pattern display a wide range of values from $A > 0.05$ to $A \simeq 1$ with $\langle A \rangle \simeq 0.4$.

The comparison of the rich variety of network burst sizes in the different configurations studied is illustrated in the boxplot Fig. 1C. For rat, a Student's t-test was used to verify that burst sizes distributions between control and PDMS squares were significantly different. In the boxplot, comparing the two different mouse configurations, the control shows an average population activity of $\langle A \rangle \simeq 0.34$, which differs from the squares, $\langle A \rangle \simeq 0.16$. Although this difference is less pronounced than in the rat cultures, it is significant ($p < 0.05$).

Another important observation from the boxplot analysis is that the mouse control does not exhibit the coherent behavior seen in the contol rat cultures, showing a very diverse burst size distribution. This could imply that the connectivity of mouse and rat cultures differs, or that their neurons operate with different dynamics.

B. Power spectrum

Given a time series, we can separate the signal into the weighted sum of sinusoidal waves through the Fourier Transform. This allows us to represent the amplitude of each component against its frequency, yielding the power spectrum of the signal. By taking the logarithm of amplitude and power, we obtain the logarithmic power spectrum which shows the relative importance of each frequency component within the overall signal.

In this study, we aimed to investigate whether the power spectrum could serve as an effective method to prove the richness and variability of neuronal cultures. The Log-log power spectrum density plots in Fig. 2 represent all the signals revealing the characteristic frequencies contained within each signal. In this sense, the power spectrum seems qualitatively similar between configurations and it is difficult to draw conclusions, indicating that both rat and mouse systems seem to behave similarly. Both cases are, however, very different from a 'uniform', on-off periodic signal that we plot as reference, indicating that neuronal cultures are more than a simple clock. Some differences, however, can be observed in the control case, with the rat having a stronger presence varied frequencies than mouse.

Having the power spectrum analysis, we can evaluate if it could be used to characterize possible avalanches in the systems and if, in case there are any, a free scale behavior would be possible to detect. However, it is important to clarify that we have results for only one decade in the frequency range which, in avalanche studies, is not enough to carry out advanced analyses such as a power law fit. The results could be interesting if the power spectrum could be adjusted to a power law in, at least, two decades. If we wanted to discuss this possibility using the power spectrum analysis, we should at least double the duration of the recordings and, also, to analyze more sets of data to have better statistics.

C. Front velocity propagation

Once the network bursts are detected, and using Dr. Soriano's software, the spatiotemporal color map of each burst can be represented (Fig. 3A). The selected bursts

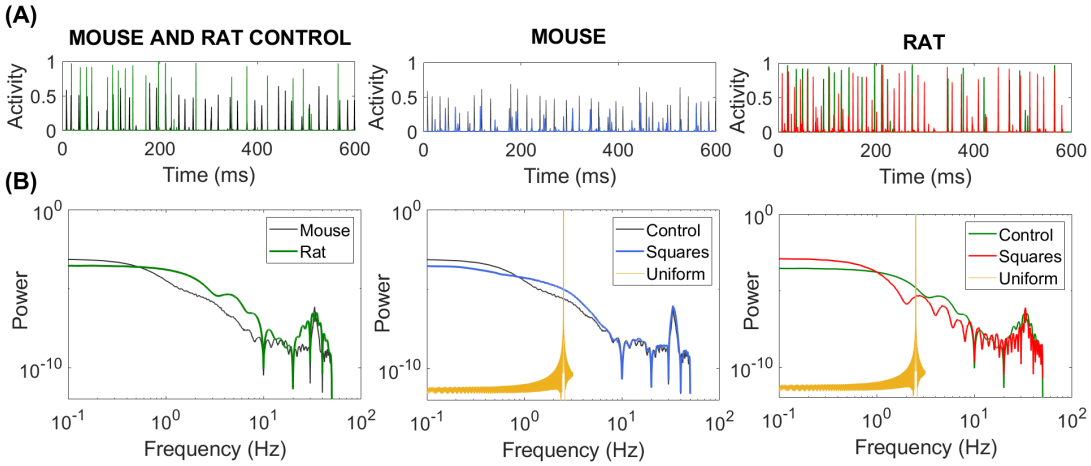

FIG. 2: Power spectrum analysis. **(A)** Comparison of signals between studied systems used to perform the power spectrum analysis. **(B)** Log-log representation of the power spectrum of the signals. The yellow line represents a uniform signal (sinusoidal) used as a reference, which clearly exhibits a peak at its characteristic frequency.

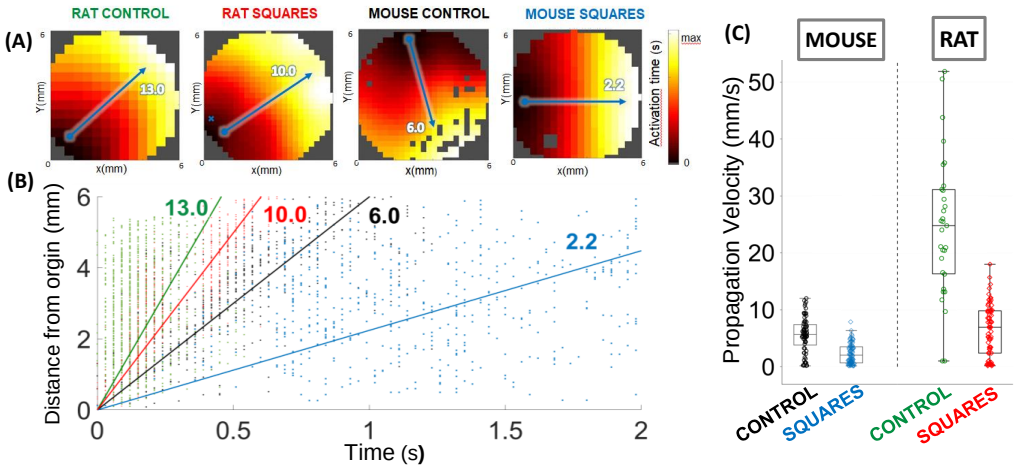

FIG. 3: Velocity of burst propagation analysis. **(A)** Examples of spatiotemporal patterns for one burst in each of the four studied systems. The color indicates the activation time, with the darker regions representing the initiation zone of the burst and white regions indicating the end. Grey regions are considered not activated during the recording. **(B)** Regression adjustment of the burst presented in (A), assuming that the wavefront propagates as a circular wave. **(C)** Distribution of the propagation velocity for all the burst detected in recordings from the four systems. These results include data from two different sets of experiments for all four systems.

present a quasi-circular front propagation, with the direction of each burst represented by an arrow.

Assuming a circular front allows us to compute the characteristic propagation velocity through linear regression of the time-distance values for each ROI, as shown in Fig. 3B. The obtained regression coefficients are typically $R > 0.65$. For rat cultures, the velocity values obtained decrease from $v \simeq 25$ mm/s in the control to $v \simeq 10$ mm/s in squared patterns; for mouse, they decrease from $v \simeq 6$ mm/s in the control to $v \simeq 2.2$ mm/s in the squared patterns. This also gives us information about the alterations in propagation velocity that presents primary mouse cultures in comparison to primary rat cultures.

A boxplot summarizing the distribution of the propagation velocities for all detected bursts in the studied configurations is presented in Fig. 3C. The results observed are consistent with the global behavior of the configurations. In both mouse and rat cultures, introducing a spatial constraint that breaks the system's isotropy leads to a decrease in velocity propagation, by a factor 2.5 in both cases. Additionally, it is clear that mouse cultures cannot reach the high velocities observed in rat control cultures, suggesting that mouse cultures may have a lower density of connections or shorter axons.

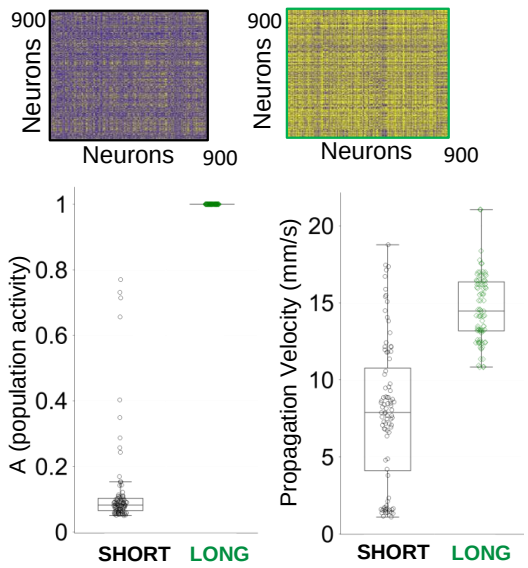

FIG. 4: Simulation results from the M. Izhikevich model. **(A)** Connectivity matrix for the two simulated systems, with connectivity radii of 2.1 mm (left, 'short' axons) and 3 mm right, 'long' axons), respectively. **(B)** Distribution of network fraction activation (left) and distribution of bursts propagation velocities (right).

D. Simulation Results

In order to explore this last hypothesis, numerical simulations were performed to demonstrate how axonal length could influence the dynamics of the system. The simulations produced a raster plot, enabling us to apply the same analytical methods as previously explained in this work.

After extensive explorations, we analyzed the data using a typical distance between connected neurons of $r = 2.1$ mm and $r = 3$ mm. These values represent the boundaries where the system transitions from being non-coherent to becoming completely synchronous, respectively.

In Fig. 4A, the connectivity matrices of the two configurations are shown, illustrating that lower connectivity range results in fewer connections. Consequently, the raster plot for the shorter connectivity range exhibits less coherent behavior, which is reflected in a wider range of population activity as presented in Fig. 4B, left. For the $r = 3$ mm data, we obtained a mean population activity of $\langle A \rangle = 1$, while for $r = 2.1$ mm, $\langle A \rangle = 0.08$.

The boxplot presenting the distribution of propagation velocities for the detected bursts in the simulation shows that the obtained results qualitatively match the experimental analysis. This suggests that the hypothesis regarding the influence of axonal length on connectivity could be valid and may partially explain the different behaviors observed in mouse and rat cultures.

IV. CONCLUSIONS

Our experimental analysis confirms that imposing spatial constraints during the growth of neuronal cultures enhances the richness of network dynamics in both rat and mouse species, highlighting the potential of such research to advance our understanding of the complexity of the human brain.

Additionally, a comparative study between rat and mouse cultures reveals distinct behaviors: rat cultures exhibit significantly higher synchrony, making them excellent experimental controls, while mouse cultures display a much richer dynamic profile, offering a more complex system for further exploration. The results from our simulations suggest that these species-specific differences may be attributed to variations in axon lengths. Future research should investigate how the density of connections impacts these systems through additional simulations.

Acknowledgments

I would like to express my sincere gratitude to my supervisor Dr. Soriano for introducing me to this field of study and for providing invaluable guidance throughout this journey. I also wish to thank Mireia for her unwavering support. Finally, I extend my heartfelt thanks to all my friends and family for their continuous encouragement over the years.

[1] J. Soriano, *Neuronal cultures: Exploring biophysics, complex systems, and medicine in a dish*. Biophysica, **3**(1), 181-202 (2023).

[2] J. Orlandi et al. *Noise focusing and the emergence of coherent activity in neuronal cultures*. Nature Phys, **9**, 582–590 (2013).

[3] Estévez-Priego et al., *Long-term calcium imaging reveals functional development in hiPSC-derived cultures comparable to human but not rat primary cultures*. Stem Cell Reports (2022).

[4] M.Montalà-Flaquer et al., *Rich dynamics and functional organization on topographically designed neuronal networks in vitro*. iScience **25**, 12 (2022).

[5] E. M. Izhikevich, *Simple model of spiking neurons*. IEEE Trans. Neur. Net. **25**(6), 1569-1572 (2003).

[6] Tibau,E., Valencia,M., & Soriano,J. *Identication of neuronal network properties from the spectral analysis of calcium imaging signals in neuronal cultures*. Frontiers in neural circuits, **7**, 199 (2013).